scientific reports

OPEN

High performance visible-SWIR flexible photodetector based on large-area InGaAs/InP PIN structure

Xuanzhang Li[1,2], Junyang Zhang[1,2], Chen Yue[1,2], Xiansheng Tang[3], Zhendong Gao[1,2], Yang Jiang[1,4], Chunhua Du[1,4,5], Zhen Deng[1,4,5✉], Haiqiang Jia[1,4,6], Wenxin Wang[1,4,6] & Hong Chen[1,4,5,6]

Mechanically flexible optoelectronic devices and systems can enable a much broader range of applications than what their rigid counterparts can do, especially for novel bio-integrated optoelectronic systems, flexible consumer electronics and wearable sensors. Inorganic semiconductor could be a good candidate for the flexible PD when it can keep its high performance under the bending condition. Here, we demonstrate a III–V material-based flexible photodetector operating wavelength from 640 to 1700 nm with the high detectivity of 5.18×10^{11} cm·Hz$^{1/2}$/W and fast response speed @1550 nm by using a simply top-to-down fabrication process. The optoelectrical performances are stable as the PDs are exposed to bending cycles with a radius of 15 mm up to 1000 times. Furthermore, the mechanical failure mode of the PD is also investigated, which suggests that the cracking and delamination failure mode are dominant in bending up and bending down direction, respectively. Such a flexible III–V material-based PD and design with stable and high performance could be a promising strategy for the application of the flexible broad spectrum detection.

Emerging application of mechanically flexible optoelectronic devices have flourished in the fields of flexible imaging/displays[1–5], sensors[6–8], short-reach data communications[9–11], solar cell[12–14] and so on. As an indispensable component of flexible optoelectronic systems, flexible photodetectors (PDs) have been extensively studied and achieved breakthroughs in nanrrow band region photoresponse: ultraviolet (UV), visble (Vis), near infrared (NIR) and broadband photoresponse. A great progress has been achieved for visible or near IR organic-based PDs, but there are several key bottlenecks, such as large bandgap, weak absorption, and poor charge generation in the NIR region, resulting in poor performance[15–17]. In recent years, significant progress has been made in multispectral PDs based on inorganic material combined with organic substrates, which makes full use of the high performance of inorganic materials and the mechanical flexibility of organic materials[18–22]. Flexible UV PDs applied ZnO[23,24], InGaZnO (IGZO)[25] and Ga_2O_3[26] with wide bandgap illustrate favorable photoresponse performance and flexibility. The inorganic semiconductor nanowires (NWs)[27–29] and 2D materials[30] such as graphene[31–34] and thin transition metal dichalcogenide (TMDCs)[18,35] have also been applied in the flexible PDs and great progress have been achieved at the UV to NIR range because of their unique electronic structure, easy fabrication, broad spectra absorption and flexibility. Especially, the transition metal dichalcogenide (TMDCs) based on organic substrate, such as MoS_2 on PET, WSe_2 or MoS_2/WSe_2 on paper, provide advanced flexible visible detectors with high responsivity and quantum efficiency, the preparation scheme has low cost and large device preparation area. Moreover, broadband photodetection has been achieved in TMDCs[18,36], IGZO[37] and Si-based material[38], which enhances the absorption of light by the decoration on surface with dissimilar superstructure or nanostructure. However, the flexible photodetection realized with above material is able to covers UV, Vis and NIR, but has no response to short-wave infrared (SWIR). The response time of the PDs mentioned above

[1]Key Laboratory for Renewable Energy, Beijing Key Laboratory for New Energy Materials and Devices, Beijing National Laboratory for Condensed Matter Physics, Institute of Physics, Chinese Academy of Sciences, Beijing 100190, China. [2]University of Chinese Academy of Sciences, Beijing 100049, China. [3]Laser Institute, Qilu University of Technology (Shandong Academy of Sciences), Jinan 250014, China. [4]Center of Materials and Optoelectronics Engineering, University of Chinese Academy of Sciences, Beijing 100049, China. [5]The Yangtze River Delta Physics Research Center, Liyang 213000, China. [6]Songshan Lake Materials Laboratory, Dongguan 523808, China. ✉email: zhen.deng@iphy.ac.cn
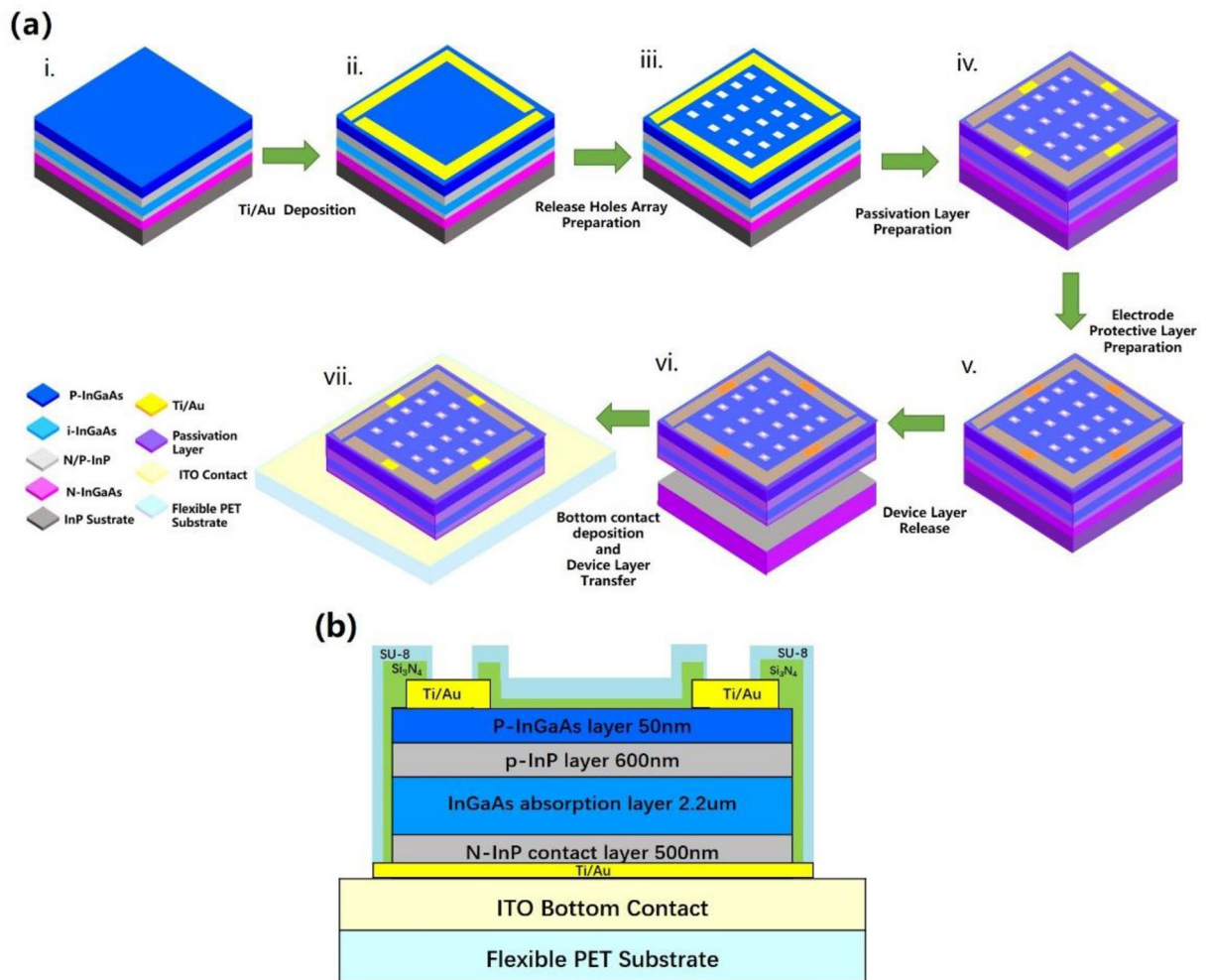
Figure 1. Device fabrication: (**a**) A flow chart for fabrication process: (i) Material growth of InGaAs PIN PD, (ii) Deposition of Up-contact metal frame. (iii) Preparation of release holes array, (iv) Preparation of passivation layer, (v) Preparation of electrode protective layer, (vi) Peeling off the InGaAs PIN membranes, (vii) Deposition of bottom contact and transfer of devices. (**b**) Cross-sectional structure of a fabricated InGaAs PIN flexible PD based on ITO-PET flexible substrate.

exceeds millisenconds (ms)[35], which is incapable to the application in high-speed detection, such as flexible communication equipment, biological sign detection, etc.

As we know, InGaAs alloy is a key component in the active regions of high-speed electronic devices[39], infrared photodetector[40] and lasers[41]. The $In_xGa_{1-x}As$ photodetector could be optimized for any wavelength with in a spectral range of 0.4 μm-3.6 μm. $In_{0.53}Ga_{0.47}As$ is lattice-matched to InP. The bandgap of $In_{0.53}Ga_{0.47}As$ is 0.74 eV, covering 1310 nm and 1550 nm low-loss communication application wavelengths. The electrons mobility of $In_{0.53}Ga_{0.47}As$ is 12,000 cm^2/Vs, which is closed to 10 times of that of Si. Combined with the current mature manufacturing technology of III–V semiconductor devices, $In_{0.53}Ga_{0.47}As$/InP PD has been widely applied and commercialized in the night vision, inspection, agricultural sorting, and so on. Thus, in this work, we have demonstrated the flexible InGaAs membrane PD with the detectivity of 5.18×10^{11} cm·Hz$^{1/2}$/W by lifting off epitaxial layers from their native substrates using a sacrificial layer and transferring them onto a flexible host carrier. A sidewall passivation is applied to simplify InGaAs PD fabrication process, and large-area flexible PDs with operating wavelength from 640 to 1700 nm are obtained, the response speed to SWIR at 1550 nm is fast enough to reach the MHz response level. Furthermore, the optoelectrical performance of such flexible PDs keeps stable in bending state and the physical mechanism is also studied in details. As a III–V materials based flexible PD with the conventional high performance of the rigid PDs, one can envision its role for the operation from visible light to short wavelength IR in the novel bio-integrated optoelectronic systems, flexible consumer electronics and wearable sensors.

Methods

The InGaAs PIN flexible PD fabrication process is schematically illustrated in Fig. 1a. The process combines material growth and device fabrication. The process of device fabrication includes seven steps: constructing metal frame, etching out the release holes, fabricating the passivation layer, coating the electrode protective layer,
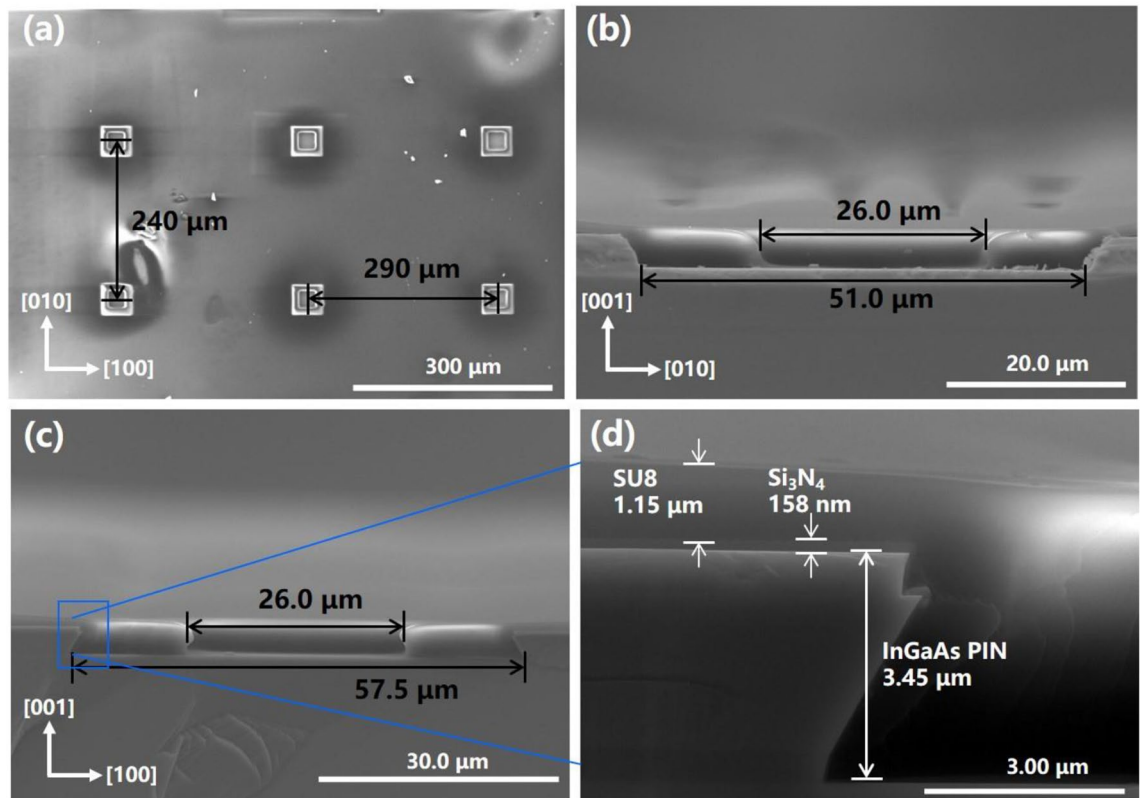
Figure 2. SEM image of etch holes in fabricated InGaAs PD based on the InP substrate: (**a**) The surface of the etch holes array. (**b,c**) The cross section of side wall covered with composite passivation layer in [100] and [010] direction. (**d**) A magnified view of a side wall of the outline area on the left shows side wall covered with Si_3N_4 (158 nm) and SU-8 (1.15 μm).

peeling off the membranes, depositing the bottom electrode contact and transferring the device layers to the flexible organic substrate. Details of the flexible PD fabrication and characterization are as follows.

Material growth.　Firstly, the III–V PIN PD membranes were grown on the 2-inch InP substrate by metal organic chemical vapor deposition. The thickness for the p- and n-type InP layers were 600 nm and 500 nm, respectively. There were three lattice-matched $In_{0.53}Ga_{0.47}As$ layers in the structure, including the top 50-nm-thick p-InGaAs layer as the ohmic contact layer, the 2.2 μm-thick undoped InGaAs layer as the absorption layer, and the 500 nm-thick n-InGaAs layer between n-InP contact layer and n-InP buffer layer as the sacrificial layer. It is noted that the p-type InGaAs layer and InP layer were achieved by single MOCVD diffusion of zinc after the epitaxy. The material characterization of InGaAs PIN photodetector is shown in supplementary material.

Device fabrication.　By using micro/nano fabrication technique, a metal frame layer (20 nm/200 nm Ti/Au) was deposited on the top of the device layers and thus two 150 μm-wide metal bars formed the metal frame layer. The metal frame layer can be used as the supporting frame to increase the mechanical strength of the to-be released InGaAs-based membrane and the top contact layer for the PD devices.

　　Arrays of 40×40 μm^2 square release holes inside were patterned on the device layers in $\langle 100 \rangle$ and $\langle 010 \rangle$ directions, by selectively wet etch down to the surface of the InGaAs sacrificial layer. The release holes were prepared to facilitate the transverse wet etching of InGaAs sacrificial layer beneath the device layer. In the process of selectively wet etching, a H_2SO_4:H_2O_2:H_2O (1:8:120) solution selectively corroded InGaAs, but had no effect on InP. On the contrary, the mixed solution of HCl:H_3PO_4 (1:3) selectively etched InP but has no effect on InGaAs. Therefore, when InGaAs or InP were etched alternately with different etching solution, excessive etching could be properly performed to ensure sufficient corrosion. Based on the selective wet-etching process, the release holes were formed down to the surface of the InGaAs layer (sacrificial layer). The release holes in detail with scan electron microscopy (SEM) were shown in Fig. 2. As the etching rates of $\langle 100 \rangle$ and $\langle 010 \rangle$ direction were different[42], the periodic spacing between the release holes was designed to be 240 μm in $\langle 010 \rangle$ and 290 μm in $\langle 100 \rangle$, respectively, as shown in Fig. 2. Compared with the same spacing distances in each directions between the release holes[43,44], the different distances design ensured that the delamination could be completed simultaneously in both directions in the process of the horizontal wet etching separation. Furthermore, as can be seen in Fig. 2, during the fabrication of release holes, the side length of the square holes expanded from 40 to 57.5 μm in $\langle 100 \rangle$ direction and 51.0 μm in $\langle 010 \rangle$ direction, which causes negligible loss to the photosensitive area.
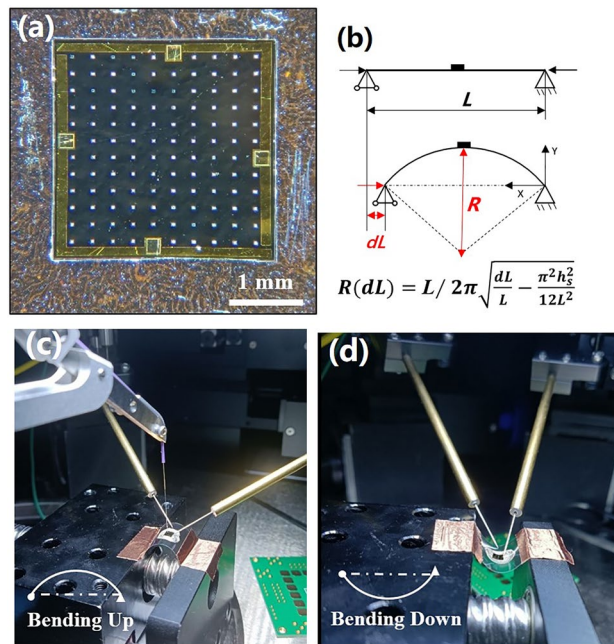
Figure 3. (**a**) Zoom-in views of a fabricated large area (3×3 mm^2) InGaAs PD on flexible PET substrate. (**b**) Schematic diagram for the measurement principle and the corresponding model. (**c,d**) A schematic diagram of fabricated flexible InGaAs PD under bending up and bending down test, respectively. The bottom left insets provide schematic illustrations of the bending geometries.

Since the absorption layer was InGaAs, the same material as the sacrificial layer, the sidewall of the InGaAs active layer in the release holes need to be protected when the selective etching solution flew to the InGaAs sacrificial layer through the release holes and undergoes etching reaction. Thus, a composite passivation layer was applied on the surface and the sidewall of the devices. According to the reference[45,46], Si$_3$N$_4$ and SU-8 both play an effective role in improving detector performance, silicon nitride (Si$_3$N$_4$) can compress dark current to promote the detectivity, SU-8 can provide better mechanical flexible support. Firstly, a 158 nm-thick Si$_3$N$_4$ layer was deposited on the top of the device layers by ICP-PECVD and then reactive ion etching was performed to open a 40×40 μm^2 square release hole in the center of each release hole formed by wet etching above, intervals between platforms and the top contact under the Si$_3$N$_4$ layer were also etched out. After that, the devices were coated with 1.15 μm SU-8, and then a 26×26 μm^2 square release hole was opened in the center of each release hole by photolithography, the intervals between platforms and the top contact under the Si$_3$N$_4$ layer were also exposed again. As shown in the Fig. 2b,c, the shape of release holes coated with SU-8 can be recognized as an inverted trapezoid in $\langle 010 \rangle$ direction and regular trapezoid in $\langle 100 \rangle$ direction. In general, the passivation layer was confirmed to prevent the InGaAs absorption layer from damage during the wet-etching of sacrificial layer.

Ti/Au top contacts were covered with photoresist, a temporary protective layer to prevent the device layers from being damaged by metal-assisted chemical etching effect[47] during the wet-etching of sacrificial layer, and the photoresist layer would be removed after the transfer. After that, the InGaAs sacrificial layer was selectively etched away by immersing the sample in a H$_2$SO$_4$:H$_2$O$_2$:H$_2$O (1:8:120) solution, and the metal framed InGaAs PIN detectors detached from the InP host substrate. Subsequently, the flexible membranes were taken out of the etching solution, and slowly dipped into deionized water to remove residual H$_2$SO$_4$ and H$_2$O$_2$.

To prepare the bottom contact, the InGaAs PIN flexible detector membranes were flipped and attached to a silicon chip coated with photoresist, then n-contact (20 nm/200 nm Ti/Au) preparation was accomplished by electron beam evaporation. Finally, InGaAs membranes lifted off from the temporary reusable substrate, and a complete InGaAs flexible PD membrane was prepared, which can be installed in any flexible circuit. In our bending experiment, the InGaAs membrane flexible PD were attached to the indium tin oxide (ITO)-PET flexible sheet (0.05 mm thick, length $L = 35$ mm) with silver conductive adhesive (about 1 μm thick), the whole flexible PD structure was shown in Fig. 1b. Micrographs of an actual device was shown in Fig. 3a.

PD characterization. The InGaAs PIN flexible PD was measured the current–voltage (I–V) in flat state and bent state at different curvature radius(R). The spectral response of the flexible PDs was carried out by a Fourier transform infrared spectrometer (Burker Vertex 70v) at room temperature in a frontside-illuminated format. All current–voltage (I–V) measurements were performed on micromanipulated probe station using a Keithley 4200 semiconductor characterization system at room temperature. An 1550 nm wavelength fiber laser with 2 μm diameter spot was used as a light source for the I-V curves under illumination characteristics. The time resolved optical response of the flexible photodetector is obtained by analyzing the transient response spectrum, the test details and schematic diagram are described in supplementary information. During the bending test, one end of
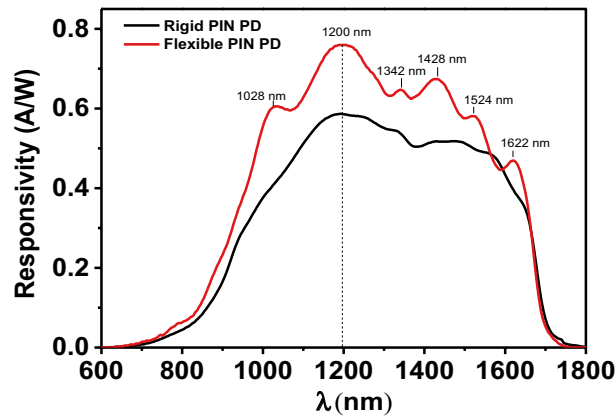
Figure 4. The response spectrum of InGaAs Flexible membrane PD and InGaAs rigid PD at 300 K.

the PET with a flexible PD was fixed and the other end was pushed forward by *dL*, the bending *R* is the function of *dL*[48], as the model shown in Fig. 3b. The bending tests of devices were performed in two direction: bending up (Fig. 3c) and bending down (Fig. 3d) for tensile and compressive strains, respectively.

Results and discussion

Figure 4 shows the spectral response ranges of the InGaAs-based membrane PD (Red line) and the InGaAs PIN rigid PD (Black line, as a counterpart) with the same area fabricated from the same epitaxy wafer. It can be clearly seen that the response wavelength of InGaAs-based membrane PD is the same with that of rigid PD in the range of 640 nm to 1700 nm, which is consistent with other reports[49,50]. The reason is that the InP contact layer of the flexible InGaAs PIN is 600 nm, and the part of the visible light can pass through the contact layer. According to the previous report[49–51], if the InP contact layer get thinner, the quantum efficiency in visible light (400–750 nm) and near-IR (750–1000 nm) wavelength region can promote, the PD can detect wavelength as short as 400 nm in the visible region. The peak of the InGaAs PIN flexible PD is 1200 nm, which is consistent with the peak position of InGaAs PIN rigid PD. It is attributed to the stability of InGaAs PIN structure even after peeling off from the InP primary substrate. In addition, peaks at 1028 nm, 1342 nm, 1428 nm, 1524 nm and 1622 nm are considered to be caused by the antireflection effect of the thickness of the SU-8/Si$_3$N$_4$ composite passivation layer on a specific wavelength, which indicates that the thickness of the passivation layer is uneven and needs to be further optimized. The peak responsivity of the InGaAs PIN flexible PD (0.76 A/W) is 28.8% higher than that of the rigid PD (0.59 A/W), which is due to the reflection of incident light by the Ti/Au bottom contact, thus enhancing the absorption and promotes the application of present device for high resolution photodetection.

Figure 5a,b shows the dark current and photocurrent density (J) of the InGaAs membrane flexible PDs in flat condition under various incident optical powers at 1550 nm. It can be clearly seen that the PDs exhibit typical rectifying characteristics, indicating an excellent quality of the PIN junction. The dark current density is approximately 2.50 μA/cm^2 at −0.1 V, and there is a gradual increase of the dark current density at the reverse bias region, which could result from the band-to-band tunneling mechanism[52]. A high sensitivity (i.e., the ratio between dark and photocurrent density) of larger than 1.57×10^8 is achieved at 1550 nm. To obtain the information about inhomogeneities at interface of device, from the slope of the V versus ln(J) plot at 300 K in the darkness, the ideality factor n is calculated as followed[36,53]:

$$ \text{n} = \frac{q}{k_B T} \frac{dV}{d(\ln(JA))} \tag{1} $$

where *q*, k_B, *T*, *J*, and *A* denote electron charge, the Boltzmann constant, operating temperature, dark current density, the effective area of the device, respectively. The ideality factor is 4.46 at 0 V. The value, greater than 1, shows the device suffers from the inhomogeneities, which is due to the poor contact between the bottom Ti/Au contact and ITO.

In addition, the PD exhibits a linear response with the excitation power increasing from 20 to 275 μW, as shown in Fig. 5c, indicating that the photogenerated carriers are dominant[54,55]. The responsivity (R_i) within the range is 0.53 A/W at −0.1 V, corresponding to an external quantum efficiency (EQE) of 42.46%. The Johnson noise limited detectivity D* of the device is calculated according to Refs.[56,57]:

$$ D^* = \frac{q\lambda \cdot EQE}{hc} \left[2qJ + \frac{4k_B T}{RA} \right]^{-\frac{1}{2}} \tag{2} $$

where *q*, *λ*, *h*, *c*, k_B, *T*, *J*, *R* and *A* denote electron charge, laser wavelength, the Planck constant, velocity of light, the Boltzmann constant, operating temperature, dark current density, differential resistance and the effective area of the device, respectively, and it can be extracted from the dark current curve that the R$_0$A of the membrane PD is 2.37×10^5 Ω cm^2. As a result, the detector exhibits a room temperature D* of 5.18×10^{11} cm·Hz$^{1/2}$/W @1550 nm at −0.1 V, whose performance is the same level with the rigid InGaAs SWIR photodetectors[58,59].
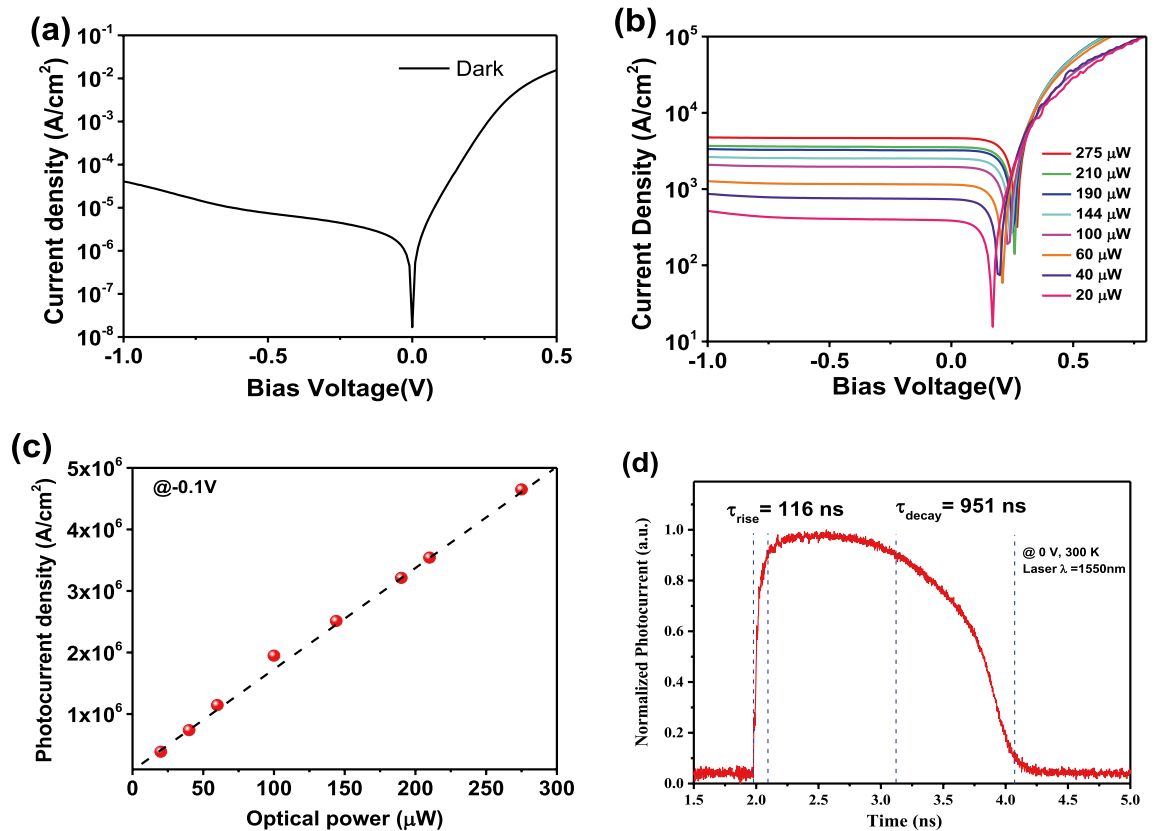
Figure 5. J–V responses of the InGaAs flexible detector under flat condition: (**a**) At darkness and (**b**) Different input optical power levels. (**c**) Photocurrent (PC) as a function of the optical power, the solid line represents a linear fitting of the experimental data. (**d**) Transient response spectrum of the detector under 0 V, inspired by a femtosecond laser ($\lambda = 1550$ nm, P = 200 μW with 100 fs pulse width).

Figure 5d shows the normalized transient response spectrum of the flexible PD, measured at 0 V with 1550 nm laser under a fixed optical power (200 μW). The rise time of the response is 116 ns and the decay time is 951 ns. Due to the slight lattice mismatch or arisen from the InGaAs/InP hetero-interface, two defects with the activation energy of 0.28 eV and 0.15 eV below the conduction band edge are formed and called deep level defect states (DLDS)[60–62]. The DLDS act as additional charge trapping centers of photo generated carriers. As the detectors is illuminated, the electron–hole pairs are generated, then the photo generated electrons are captured in the DLDS before reaching the Ti/Au electrodes. The defect states are charged under illumination until filled, then the electrons in the conduction band are extracted to the electrodes, a new static equilibrium is attained and channel current reaches its maximum value. As the illumination is off, electron trapped in the defect states are released and the equilibrium changes, the channel current decays to its original value[63]. Hence, the process of the defect state filling and the release increase the response time of the flexible detector.

The InGaAs PIN flexible prototype photodetector possesses high surface-to-volume ratio, the surface of the device tend to absorb large number of atmospheric molecular, such as water vapor, oxygen, carbon dioxide absorbed during the device fabrication and testing. The According to the oxygen-assisted mechanism[36,53]:

$$O_2(g) + e^- \rightarrow O_2^-(ad)(Darkness) \tag{3}$$

$$O_2^-(ad) + h^+ \rightarrow O_2(g)(Illumination) \tag{4}$$
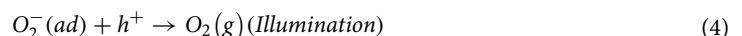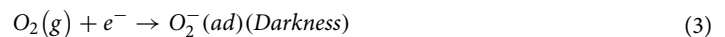
Under the dark condition, the absorbed oxygen atoms in the devices absorb electrons from active material of the device and become negatively charged, as shown in Eq. (3). As the detector is inspired, the photo-generated holes are captured in oxygen absorbed on surface defect states, as shown in Eq. (4), then the holes are released from the oxygen when the illumination is off. As the process of the deep level defect states trapping and releasing photo-generated electrons, the interaction between oxygen and photo-generated holes leads to a prolonged response time. Besides, the high resistance of poor ohmic contact and operating circuit could increase the response time[40]. To shorten the response time of the InGaAs PIN flexible PD, the growth condition and the device fabrication should be optimized further. In general, the results suggest the InGaAs PIN flexible PD is fast enough to reach the MHz response level.

In order to study the flexible optoelectrical characteristics, the related characterization for the membrane PDs are performed under the bent condition, while the flat condition is referred as the counterpart. Figure 6 shows the PD's dark current density and photoresponse in their flat and bent up/down state. It should be noted that
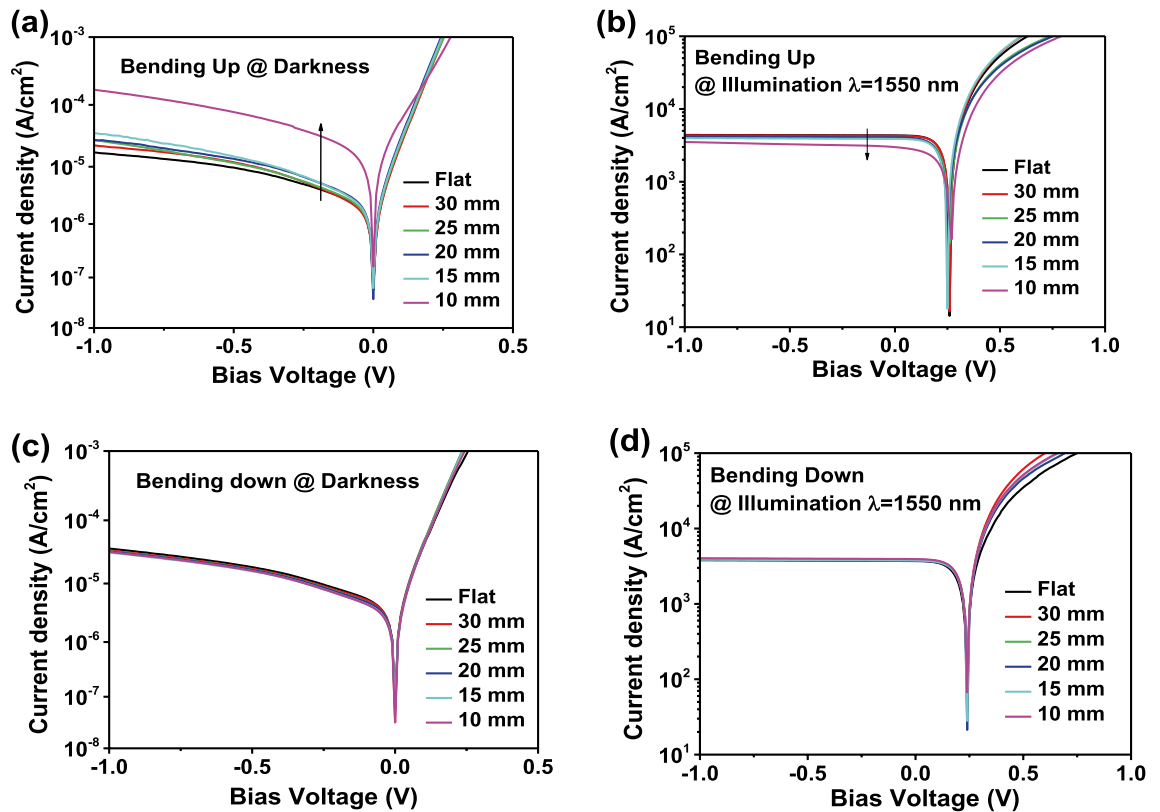
Figure 6. Device characterization under bent conditions: J–V responses of the detector under bending up and down condition. At darkness: (**a,c**) and Illumination: (**b,d**) at 1550 nm (P = 230 µW).

the dark current density increases gradually under bent down condition (Fig. 6a) as R reduces. Especially when the R is reduced from 15 to 10 mm, the dark current density increases by 5 times. Meanwhile, the phototcurrent density of the device is stable when the radius reduced from 30 to 15 mm, but decreases by 28% as R is 10 mm. Compared with the bending up condition, the dark current and photocurrent both remain stable under bending down condition, as the radius reduces from 30 to 10 mm.

Furthermore, the failure mode of such PDs have been studied deeply. Optical microscope images as shown in Fig. 7 suggest the failure modes of the flexible InGaAs detectors in two bending directions are different. Under bending up condition, cracks are visible at R = 10 mm in Fig. 7a,b, the cracks form perpendicular to the forward direction of dL and propagate from one release hole to another one. The cracks lead to the increase of surface leakage current and the decrease of photocurrent. In addition, once the craking mode occurs, the performance degradation is irreversible. In bending down direction, instead of cracking, we observed that the membrane buckled upward via local delamination from the adhesive at R = 10 mm, as shown in Fig. 7c. The delamination reduces the strain in the membrane thereby preventing the cracking failure mode even at smaller bending radius. Therefore, the device can be bent down to R = 10 mm while keeping the integrity and stable photo response of the device. As the bending radius decreases further, the delamination continues to expand, as shown in Fig. 7d. Even if the bending is released, the membranes do not slip back and stay in delamination forever. Instead of the fracture strains of membranes suffering, the interfacial shear stresses are responsible for the failure behavior and the delamination failure is sensitive to the adhesion strength of film to the substrate[48]. Hence, increasing the adhesion strength of InGaAs membrane PD to PET helps to overcome delamination.

According to the study about the failure mode of bending silicon ribbons on plastic substrates, the thickness of the silicon ribbons determines the dominant failure mode of the bending mechanics. As the thickness increases, the dominant failure mode is as follows: cracking, slipping and delamination[48,64,65]. However, there are two failure modes for the InGaAs flexible PD with a fixed thickness in two bending direction. Unlike the silicon ribbon, the InGaAs flexible PD is a composite multilayer asymmetric structure, the effect of bending strain on each layer of material is different. As shown in Fig. 1b, SU-8 layer, Si_3N_4 layer and the metal contact coated on the InGaAs PIN membrane structure, asymmetrically from top to bottom. The failure mode is supposed to occur from one layer and transmit to the whole structure. Top and bottom thin metal contact has ductility, and its contribution to the failure membranes can be neglected. The comparison of the Young's moudlus for SU-8, Si_3N_4 and InGaAs PIN membrane is: SU-8 (3–5 GPa) < InGaAs PIN membrane (60–80 GPa) < Si_3N_4 (220–230 GPa). The failure mode is more likely to occur in InGaAs PIN membrane and Si_3N_4. Considering the thickness of the three materials, it can be assumed that, cracking failure dominated in bending up caused by thin Si_3N_4, and the delamination failure dominated in bending down caused by thick InGaAs PIN expitaxy layer. The quantitative analysis of this hypothesis can be further studied, and provide guidance for the bending performance optimization.
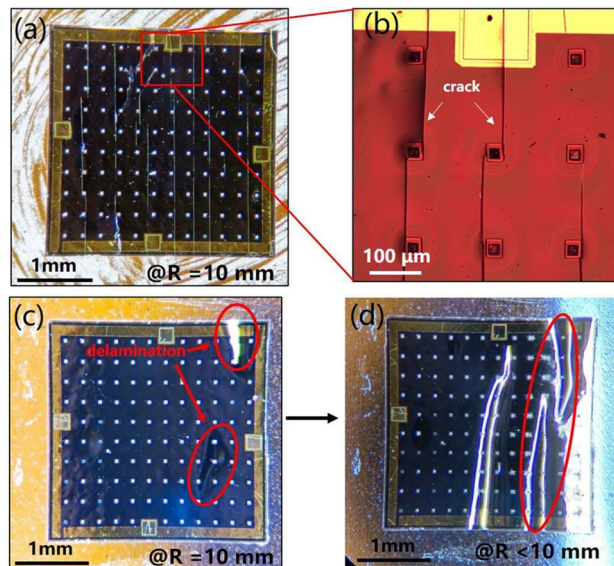
Figure 7. Microscope image of bending flexible InGaAs detector: (**a**) Bending up of R = 10 mm. (**b**) A magnified view of the outline area on the left shows the cracking failure surface. (**c**) Bending down of R = 10 mm shows the appearance of the delamination failure. (**d**) Bending up of R < 10 mm shows the expansion of the delamination failure.

In general, the ratio between dark and photocurrent density of the PDs remains stable, larger than 7×10^8 under bending up condition with R decreasing from 30 to 15 mm and bending down condition with R decreasing from 30 to 10 mm, respectively, indicating that the simplify fabrication of InGaAs PIN membrane flexible PD is feasible.

Fatigue test of the InGaAs-based flexible PD is further performed with a self-assembled slide stable system. The PD is bent on the automated slide rail for 1, 10, 100, and 1000-times bending down cycles, respectively. As shown in Fig. 8a,b, the dark and photo current density of the InGaAs PIN flexible PD are stable after 10, 100 and 1000 times bending cycles. The ratio of photo to dark current density remain more than 4×10^8, while the responsivity remains above 0.49 A/W and thus no failure occur after the bending cycle, as shown in Fig. 8c. These results suggest that such PDs have an excellent durability of the optoelectrical performance after multiple mechanical deformations. Therefore, it could be believed that such gratifying robustness of the InGaAs-based flexible PD with the simplified fabrication process is promising to be applied in the flexible optoelectronic field.

Conclusion

In this paper, we have demonstrated the InGaAs-based membrane flexible PD with the detectivity of 5.18×10^{11} cm·Hz$^{1/2}$/W by a top-to-down fabrication technique using a sacrificial layer and transferring them onto a flexible host carrier. A side wall passivation with SU-8 and Si_3N_4 is applied to simplify InGaAs PD fabrication process. And a large-area flexible PD with operating wavelength from 640 to 1700 nm is obtained and the response speed reaches MHz level. Furthermore, the results reveal that the over-all optoelectrical performance of such flexible PDs keeps stable in bending state. In addition, fatigue test suggests that cracking and delamination modes dominates in bending up and down conditions, respectively. We believe that the demonstrated III–V material-based flexible PD with the high performance of the rigid PD is step forward in merging mature compound semiconductor technology and flexible optoelectronic device with simple design and high performance for broad spectrum detection.
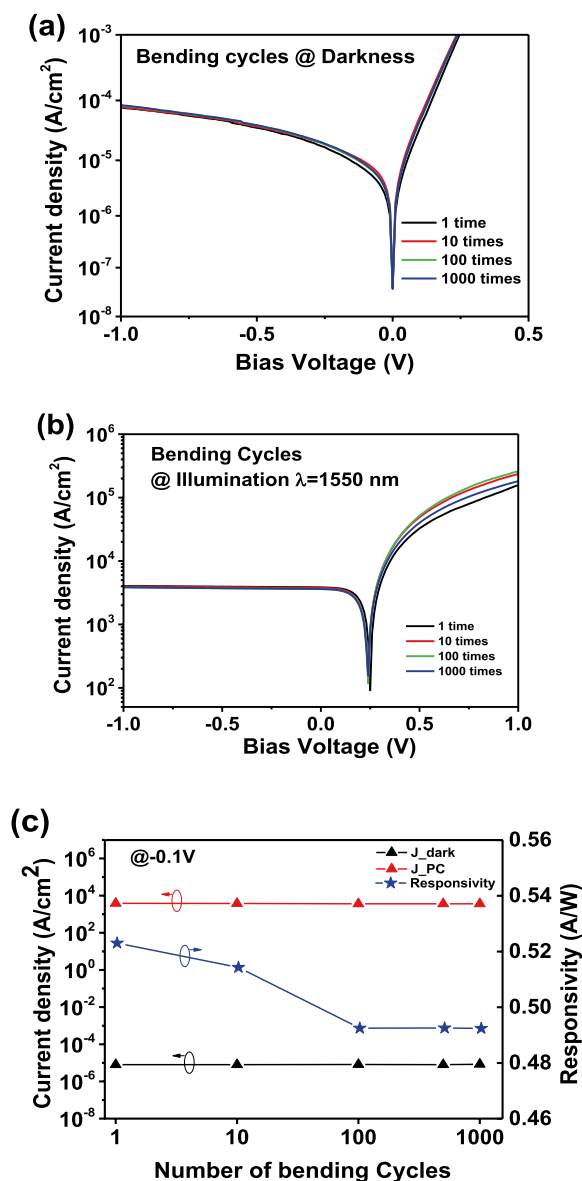
Figure 8. Devices characterization after multiple bending down cycle of 1, 10, 100, 1000 times (a radius of R = 15 mm): (**a**) Dark density of the devices; (**b**) Photocurrent density of the devices; (**c**) Left: Dark and photocurrent (PC) density of the devices at − 0.1 V; Right: Responsivity of the device at 1550 nm (P = 230 μW) at − 0.1 V.

Data availability
All data generated or analysed during this study are included in this published article (and its Supplementary Information files).

References
1. Forrest, S. R. The path to ubiquitous and low-cost organic electronic appliances on plastic. *Nature* **428**, 911–918 (2004).
2. Chien, L.-C., Okuda, Y., Lee, S.-D., Fujieda, I. & Wu, M.H. In *Advances in Display Technologies II* (2012).
3. Seo, J.-H. *et al.* A simplified method of making flexible blue LEDs on a plastic substrate. *IEEE Photonics J.* **7**, 1–7 (2015).
4. Park, J. *et al.* Research on flexible display at Ulsan National Institute of Science and Technology. *NPJ Flex. Electron.* **1**, 1–13 (2017).
5. Choi, M. K., Yang, J., Hyeon, T. & Kim, D.-H. Flexible quantum dot light-emitting diodes for next-generation displays. *Npj Flex. Electron.* **2**, 1–14 (2018).
6. Park, J. *et al.* Giant tunneling piezoresistance of composite elastomers with interlocked microdome arrays for ultrasensitive and multimodal electronic skins. *ACS Nano* **8**, 4689–4697 (2014).

7. Salvatore, G. A. *et al.* Biodegradable and highly deformable temperature sensors for the internet of things. *Adv. Funct. Mater.* **27**, 1702390 (2017).
8. Ha, M., Lim, S. & Ko, H. Wearable and flexible sensors for user-interactive health-monitoring devices. *J. Mater. Chem. B* **6**, 4043–4064 (2018).
9. Bosman, E. *et al.* Highly reliable flexible active optical links. *IEEE Photonics Technol. Lett.* **22**, 287–289 (2010).
10. Dangel, R. *et al.* Development of versatile polymer waveguide flex technology for use in optical interconnects. *J. Lightwave Technol.* **31**, 3915–3926 (2013).
11. Li, L. *et al.* A fully-integrated flexible photonic platform for chip-to-chip optical interconnects. *J. Lightwave Technol.* **31**, 4080–4086 (2013).
12. Fu, X., Xu, L., Li, J., Sun, X. & Peng, H. Flexible solar cells based on carbon nanomaterials. *Carbon* **139**, 1063–1073 (2018).
13. Shin, D. H., Jang, C. W., Lee, H. S., Seo, S. W. & Choi, S. H. Semitransparent flexible organic solar cells employing doped-graphene layers as anode and cathode electrodes. *ACS Appl. Mater. Interfaces* **10**, 3596–3601 (2018).
14. Fan, Z. *et al.* Three-dimensional nanopillar-array photovoltaics on low-cost and flexible substrates. *Nat. Mater.* **8**, 648–653 (2009).
15. Tordera, D. *et al. Organic Flexible Electronics* 575–597 (Elsevier, 2021).
16. Xu, H. *et al.* Flexible organic/inorganic hybrid near-infrared photoplethysmogram sensor for cardiovascular monitoring. *Adv. Mater.* **29**, 1700975 (2017).
17. Khan, Y. *et al.* A flexible organic reflectance oximeter array. *Proc. Natl. Acad. Sci. USA* **115**, E11015–E11024 (2018).
18. Patel, M., Pataniya, P. M. & Sumesh, C. K. Enhanced photoresponse by plasmon resonance in Ni-WS2/Si photodiode. *Mater. Res. Bull.* **145**, 111518 (2022).
19. Djeffal, F. *et al.* Highly efficient and low-cost multispectral photodetector based on RF sputtered a-Si/Ti multilayer structure for Si-photonics applications. *J. Alloys Compd.* **876**, 160176 (2021).
20. Benyahia, K. *et al.* Self-powered photodetector with improved and broadband multispectral photoresponsivity based on ZnO–ZnS composite. *J. Alloys Compd.* **859**, 158242 (2021).
21. Mahdi, M. S. *et al.* High performance and low-cost UV–Visible–NIR photodetector based on tin sulphide nanostructures. *J. Alloys Compd.* **735**, 2256–2262 (2018).
22. Dhanabalan, S. C., Ponraj, J. S., Zhang, H. & Bao, Q. Present perspectives of broadband photodetectors based on nanobelts, nanoribbons, nanosheets and the emerging 2D materials. *Nanoscale* **8**, 6410–6434 (2016).
23. Zhang, Y. *et al.* Flexible transparent high-voltage diodes for energy management in wearable electronics. *Nano Energy* **40**, 289–299 (2017).
24. Zhang, Y. et al. Flexible Transparent Field-Effect Diodes Fabricated at Low-Temperature with All-Oxide Materials. *Advanced Electronic Materials* **2** (2016).
25. Huo, W. *et al.* Flexible transparent InGaZnO thin-film transistors on muscovite mica. *IEEE Trans. Electron. Devices* **66**, 2198–2201 (2019).
26. Sui, Y., Liang, H., Huo, W., Wang, Y. & Mei, Z. A flexible and transparent β-Ga2O3 solar-blind ultraviolet photodetector on mica. *J. Phys. D: Appl. Phys.* **53**, 504001 (2020).
27. Zhe, *et al.* Fabrication of high-quality ZnTe nanowires toward high-performance rigid/flexible visible-light photodetectors. *Opt. Express* **21**, 7799 (2013).
28. Chen, G. *et al.* High performance rigid and flexible visible-light photodetectors based on aligned X(In, Ga)P nanowire arrays. *J. Mater. Chem. C* **2**, 1270–1277 (2014).
29. Dahiya, A. S. *et al.* High-performance printed electronics based on inorganic semiconducting nano to chip scale structures. *Nano Converg.* **7**, 33 (2020).
30. De Fazio, D. *et al.* High responsivity, large-area graphene/MoS2 flexible photodetectors. *ACS Nano* **10**, 8252–8262 (2016).
31. Kang, P., Wang, M. C., Knapp, P. M. & Nam, S. Crumpled graphene photodetector with enhanced, strain-tunable, and wavelength-selective photoresponsivity. *Adv. Mater.* **28**, 4639–4645 (2016).
32. Goossens, S. *et al.* Broadband image sensor array based on graphene–CMOS integration. *Nat. Photonics* **11**, 366–371 (2017).
33. Yousefi, R. *et al.* Effect of annealing temperature and graphene concentrations on photovoltaic and NIR-detector applications of PbS/rGO nanocomposites. *Ceram. Int.* **42**, 15209–15216 (2016).
34. Noumbe, U. N. *et al.* Reconfigurable 2D/0D p-n graphene/HgTe nanocrystal heterostructure for infrared detection. *ACS Nano* **14**, 4567–4576 (2020).
35. Dong, T., Simões, J. & Yang, Z. Flexible photodetector based on 2D materials: processing, architectures, and applications. *Adv. Mater. Interfaces* **7**, 1901657 (2020).
36. Patel, M., Pataniya, P. M., Late, D. J. & Sumesh, C. K. Plasmon-enhanced photoresponse in Ag-WS2/Si heterojunction. *Appl. Surf. Sci.* **538**, 148121 (2021).
37. Wei, S. *et al.* Flexible quasi-2D perovskite/IGZO phototransistors for ultrasensitive and broadband photodetection. *Adv. Mater.* **32**, e1907527 (2020).
38. Jin, X. *et al.* High-performance free-standing flexible photodetectors based on sulfur-hyperdoped ultrathin silicon. *ACS Appl. Mater. Interfaces* **11**, 42385–42391 (2019).
39. Zhang, J., Itzler, M. A., Zbinden, H. & Pan, J.-W. Advances in InGaAs/InP single-photon detector systems for quantum communication. *Light Sci. Appl.* **4**, e286–e286 (2015).
40. Kaniewski, J. & Piotrowski, J. InGaAs for infrared photodetectors. *Phys. Technol. Opto-Electron. Rev.* **12**, 139–148 (2004).
41. Tångring, I. *et al.* 1.58μm InGaAs quantum well laser on GaAs. *Appl. Phys. Lett.* **91**, 221101 (2007).
42. Pasquariello, D. *et al.* Selective undercut etching of InGaAs and InGaAsP quantum wells for improved performance of long-wavelength optoelectronic devices. *J. Lightwave Technol.* **24**, 1470–1477 (2006).
43. Kiefer, A. M. *et al.* Si/Ge junctions formed by nanomembrane bonding. *ACS Nano* **5**, 1179–1189 (2011).
44. Yang, W. *et al.* Large-area InP-based crystalline nanomembrane flexible photodetectors. *Appl. Phys. Lett.* **96**, 121107 (2010).
45. Li, J. et al. In *AOPC 2017: Optical Sensing and Imaging Technology and Applications* (2017).
46. Kim, H. S. *et al.* Performance improvement of InAs/GaSb strained layer superlattice detectors by reducing surface leakage currents with SU-8 passivation. *Appl. Phys. Lett.* **96**, 033502 (2010).
47. Kong, L. *et al.* Damage-free smooth-sidewall InGaAs nanopillar array by metal-assisted chemical etching. *ACS Nano* **11**, 10193–10205 (2017).
48. Park, S.-I. *et al.* Theoretical and experimental studies of bending of inorganic electronic materials on plastic substrates. *Adv. Funct. Mater.* **18**, 2673–2684 (2008).
49. Andresen, B.F. et al. In *Infrared Technology and Applications XXX* (2004).
50. Andresen, B.F. et al. In *Infrared Technology and Applications XXXIV* (2008).
51. Cohen, M.J., Lange, M.J., Ettenberg, M.H., Dixon, P. & Olsen, G.H. In *LEOS '99. IEEE Lasers and Electro-Optics Society 1999 12th Annual Meeting* (1999).
52. Huang, Y. H., Chang, G. E., Li, H. & Cheng, H. H. Sn-based waveguide p-i-n photodetector with strained GeSn/Ge multiple-quantum-well active layer. *Opt. Lett.* **42**, 1652–1655 (2017).
53. Patel, M., Pataniya, P. M., Patel, V., Sumesh, C. K. & Late, D. J. Large area, broadband and highly sensitive photodetector based on ZnO-WS2/Si heterojunction. *Sol. Energy* **206**, 974–982 (2020).
54. Li, L. *et al.* High-performance flexible waveguide-integrated photodetectors. *Optica* **5**, 44 (2018).

55. An, S. *et al.* High-sensitivity and mechanically compliant flexible ge photodetectors with a vertical p–i–n configuration. *ACS Appl. Electron. Mater.* **3**, 1780–1786 (2021).
56. Haddadi, A. *et al.* High-performance short-wavelength infrared photodetectors based on type-II InAs/InAs1-xSbx/AlAs1−xSbx superlattices. *Appl. Phys. Lett.* **107**, 141104 (2015).
57. Liu, J. *et al.* InAs/InGaAs/InAlAs interband quantum well infrared photodetector (IQWIP) with cut-off response wavelength at 1.93 μm. *Appl. Phys. Express* **12**, 032005 (2019).
58. Shao, X. *et al.* Developments of high performance short-wave infrared InGaAs focal plane detectors. *Infrared Technol.* **38**, 629–635 (2016).
59. Xie, Z., Deng, Z., Zou, X. & Chen, B. InP-based near infrared/extended-short wave infrared dual-band photodetector. *IEEE Photonics Technol. Lett.* **32**, 1003–1006 (2020).
60. Vu, T. K. O., Lee, K. S., Lee, S. J. & Kim, E. K. Defect states in InP/InGaAs/InP heterostructures by current-voltage characteristics and deep level transient spectroscopy. *J. Nanosci. Nanotechnol.* **18**, 6239–6243 (2018).
61. Wang, C. et al. In *2017 China Semiconductor Technology International Conference (CSTIC)* 1–4 (2017).
62. Forrest, S. R. & Kim, O. K. Deep levels in In0.53Ga0.47As/InP heterostructures. *J. Appl. Phys.* **53**, 5738–5745 (1982).
63. Pataniya, P. *et al.* Paper-based flexible photodetector functionalized by WSe2 nanodots. *ACS Appl. Nano Mater.* **2**, 2758–2766 (2019).
64. Huang, Y., Feng, X. & Qu, B. Slippage toughness measurement of soft interface between stiff thin films and elastomeric substrate. *Rev. Sci. Instrum.* **82**, 104704 (2011).
65. Dai, L., Yin, H., Hang, C., Xue, F. & Fang, D. Transition among failure modes of the bending system with a stiff film on a soft substrate. *Appl. Phys. Lett.* **106**, 021905 (2015).

Acknowledgements

Author contributions

X.L. and Z.D. conceived the idea. X.L. conducted the device fabrication. J.Z., C.Y., X.T. and Z.G. equally to this work for assisting the sample preparation and characterization. H.C. supervised the entire research project. The manuscript was written by X.L. and Z.D. All authors have reviewed the manuscript and given their approval to the final version of this manuscript.

Competing interests

The authors declare no competing interests.

Additional information

Supplementary Information The online version contains supplementary material available at https://doi.org/10.1038/s41598-022-11946-7.

Correspondence and requests for materials should be addressed to Z.D.

Reprints and permissions information is available at www.nature.com/reprints.

Publisher's note Springer Nature remains neutral with regard to jurisdictional claims in published maps and institutional affiliations.